Creep Mechanisms vis-à-vis Power Law vs. Grain Boundary Sliding in α-β Titanium Alloys for Physics Based Prognostics

Amar Kumar[1], Alka Srivastava[1], Nita Goel[1], Avi Banerjee[2] and Ashok K Koul[2]

[1]Tecsis Corporation, 210 Colonnade Road, Ottawa, ON, K2E 7L5, Canada
[2]Life Prediction Technologies Inc., 23-1010 Polytek Street, Ottawa, ON, K1J 9J1, Canada

ABSTRACT

This work is performed in support of our continued physics-based prognostics system development using a life cycle management-expert system (LCM-ES) framework. The physical damage based modeling approach involving global behavior and localized response of a component at the microstructural level is used. The current research aims at constructing parts of a deformation mechanism map (DMM) for α-β Ti alloy. The appropriate constitutive equations are used for power law creep and grain boundary sliding mechanisms. Simulations are performed using the Newton-Raphson method using Matlab software code in order to obtain contour lines corresponding to strain rates ranging from 10^{4} to 10^{-12} over the homologous temperature ranges of 0.10 to 0.655. The dominance of power law creep and grain boundary sliding over a wider range of stresses and temperatures in Ti-64 alloy is studied. The simulation results are validated using experimental data points. The predicted contour lines in the map match fairly well. The structure-creep mechanism relationships in α-β Ti alloy under different stress, temperature and strain rate conditions are discussed.

1. INTRODUCTION

Creep deformation involving significant plastic strain accumulation in titanium alloys is the single major cause for compressor and turbine failure. It is known to occur by a number of alternative and competitive mechanisms. Creep failure resistance remains a big challenge for all high temperature design and service considerations. The problem has assumed greater significance in titanium alloys for physics based approach and analysis for the development of diagnostic prognostic and health management systems. Titanium alloys are used in a wide variety of microstructures and properties and are subjected to wide ranges of operating conditions in aeroengines (Badea et.al, 2014; Evans and Harrison, 1983; Seco and Irisarri, 2001). Deformation mechanism maps (DMM) summarize information regarding dominance of creep plasticity mechanisms in temperature and stress space varying as a function of strain rate in a given microstructure. Both creep mechanism and the strain rate are the major variables for assessing the rate of damage accumulation in physics based prognostic analysis. The DMMs are constructed with axes of normalized shear stress σ_s/μ (μ being the shear modulus) and T/T_m where T_m is the melting temperature of the alloy. This space is divided into various fields which show the regions of stress and temperature over which each deformation mechanism is dominant. (Frost and Ashby, 1982). The dominant deformation mechanisms include dislocation glide, dislocation creep and Harper-Dorn creep, power law creep (dislocation glide plus climb) and diffusion creep mechanisms, i.e., Nabarro–Herring creep and Coble creep (Frost and Ashby, 1982; Langdon, 2006; Janghorban and Esmaeili, 1991). This understanding of constructing DMMs arose from using experimental data and microstructural evidence collected on simple metals and alloys. The applicability of these concepts to complex engineering alloys is now being questioned. Instead of diffusional creep mechanisms, grain boundary sliding accommodated by different thermally activated processes is considered likely as a dominant deformation mechanism in complex engineering alloys (Janghorban and Esmaeili, 1991; Briquette et. al., 2012; Bano, Koul and Nganbe, 2014).

In physics-based prognostics, use of physically realistic damage models is a prerequisite for accurate life prediction of cold and hot section turbine components. A life cycle management-expert system (LCM-ES) framework involves the integration of both global behavior and localized response at the microstructural level (Banerjee et. al., 2013). Microstructural variability in a damage model was considered earlier for the prediction of the component reliability upfront (Banerjee et. al., 2013; Metzer and Seifert, 2012).

The primary objective of this paper is to construct a DMM for an α- β Ti alloy showing the dominance of power law creep (PLC) and grain boundary sliding (GBS) over a range of stresses and temperatures. The work emphasizes the importance of GBS mechanism leading to grain boundary cavitation and wedge cracking. The commonly used constitutive rate equations and a newly modified Matlab soft code are considered for the reconstruction of the PLC and GBS regimes. The other interest of the work is to identify the power law deviation separated from the region of power law dominance. The theoretically reconstructed DMM is further validated with experimental data points available in the literatures.

2. α- β TI ALLOY SYSTEMS

The IMI 834 is one of the latest near-α titanium alloys developed for compressor discs, blades and vanes of modern aircraft jet engines. High-temperature creep resistance is one of the prime requirements of IMI 834 since the alloy is targeted for application up to about 600°C ($T/T_m = 0.45$). The desirable microstructure of this alloy for compressor application with good combination of fatigue and creep resistance has been found to be about 15% equiaxed primary α phase embedded in transformed β matrix. The aeroengine components operating at high temperatures are prone to creep failure due to high sustained rotational speeds. Also, the components during service are frequently subjected to varying stresses and temperatures. Thus these become susceptible to localized creep or low cycle fatigue (LCF) damage, which leads to initiation of cracks early in life. Modern aircraft engines have portions of compressor that operate in the temperature range of 325°C ($T/T_m = 0.31$) to 575°C ($T/T_m = 0.44$) and have Ti alloys for the stressed rotors (Es-Soumi, 2001, Lutjering and Williams, 2007; Donachie, 2002).

The Ti-6Al-4V (Ti-64) is the most widely used and studied alloy. The aluminium stabilizes the alpha phase while the vanadium stabilizes the beta phase. These alloys can be solution treated, quenched and aged for increased strength. The microstructure of the alloy depends on its composition and heat treatment. Creep strength is not as good as most near Alpha alloys. The properties of Ti-64 vary smoothly with increasing temperature, covering the range from minus 196°C up to 750°C. Although the alloy retains useful short-term properties up to 500°C, but its properties over the longer term tend to limit its use to 300°C. The LCF behavior for Ti-64 is highly structure dependent as beta forged has the least resistance, while 10 % alpha–beta structure shows the highest resistance (Leyens and Peters, 2003; Peters et. al., 2003).

3. CREEP DEFORMATION MECHANISMS

A brief account of creep mechanisms considered in the work is discussed in order to highlight their importance and implications. The generic creep mechanisms in Ti alloys covers different sections of the map as separated by the boundaries. Fig. 1 is reproduced here from earlier work for illustratration (Janghorban and Esmaeili, 1991). The whole map is subdivided into various regime where the dominant mechanism prevails as a function of stress and temperature. The diffusional creep as well as power law creep are shown to be prevailing over $0 < T/Tm < 0.6$, however the PLC appears to be at much higher stress level. The strain rate contour lines go over different regimes depending on the stress applied and temperatures. However, earlier work did not consider the GBS mechanism.

3.1. Power Law Creep

The rate at which the dislocations can overcome a series of obstacles within the crystal determine the glide/climb rate and consequently strain accumulation (Wu, 2010). At higher temperature, movement of the dislocations become easier. Thermal activation enables edge dislocations to climb from one glide plane to another by either absorbing or emitting vacancies at a sufficient rate to bypass the obstacles. A large number of models have been proposed for PLC (Leyens and Peters, 2003; Peters et. al., 2003). The generic form of power law creep (PLC) is represented by

$$\varepsilon_{ss} = A\sigma^n \, exp\left(\frac{-Q}{RT}\right) \quad (1)$$

In general, in stress dependence 'n' is termed as stress exponent, σ is the stress and ε_{ss} is the creep strain rate. In temperature dependency, Q is the activation energy, R is the gas constant, T is temperature and A is the material dependent constant. Prediction of the value of n from first principles is not easy, but its value does depend on which mechanism is operating. Uncertainties lie with selection of appropriate values of apparent activation energy (Q) and stress exponents (n). High values of Q and n have led to confusion about rate controlling mechanisms and hence a number of models have been proposed. These anomalies have been reported for various alloy systems including titanium (Barboza et. al, 2006). However, several works on these materials have shown that the anomalous behavior can be rationalized by considering the presence of a threshold stress (σ_o) opposing creep flow and the creep rate is related to an effective stress ($\sigma - \sigma_o$), where σ is the applied stress (Badea et. al., 2014; Barboza et. al. 2006). For diffusion creep the value of exponent is approximately 1, while for deformation governed by transgranular dislocation glide/climb it is usually in the range 3-8. At high temperature, the supply of vacancies for the climb of dislocation is assumed to occur through volume diffusion resulting in values for the stress exponent, n, ranging from 3 to 5. At lower temperatures vacancy diffuses predominantly along the dislocation cores. The rate at which vacancies are supplied to or removed from the climbing dislocations is then dependent on the dislocation density

which is itself a function of the applied stress. Stress exponents of 5 to 8 are then predicted (Wu, Koul, 1999; Wu, Dickson and Koul, 1998; Wu, 2010). Unusual higher values greater than 15 are also reported (Evans and Harrison, 1983).

Power law dominated creep was reported in near α Ti duplex microstructures with 17% primary α for IMI 834 and fully transformed microstructures for IMI 829 and 685. Stress exponents are reported to be 4.2 to 5.2 for the steady-state and from 3.2 to 6.2 for the transient creep rates. The activation energy for the alloys are in the range of 300 to 345 kJ/mol. (Es-soumi 2001).

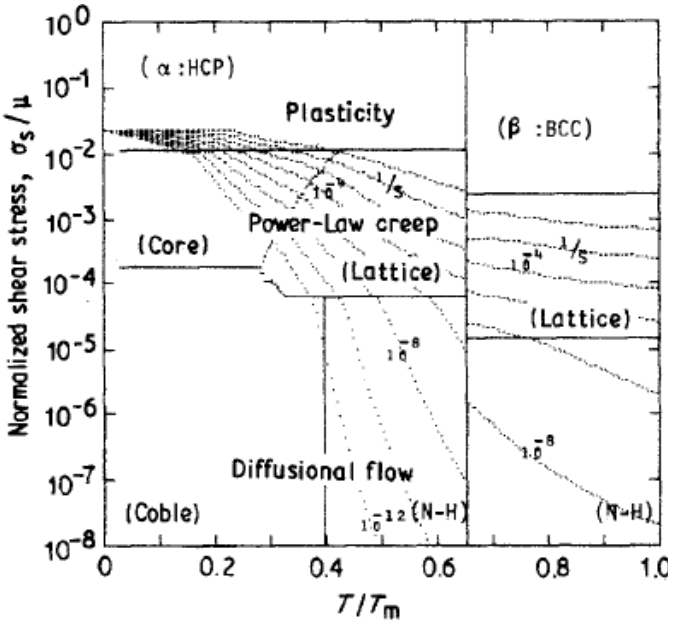

Figure 1. Illustration of dominance of various creep mechanisms in Ti-6Al alloy of grain size 100 microns (Janghorban and Esmaeili, 1991).

3.2. Grain Boundary Sliding (GBS)

At high temperature, grain boundaries tend to slide to cause creep deformation. Langdon developed a rate equation for GBS taking into account the movement of dislocations within, or adjacent to, boundary planes, through a combination of dislocation glide and climb steps (Langdon; 2006). The rate of sliding was considered to be controlled by the rate of accommodation through intragranular slip. The model showed good agreement with experimental results under creep and superplastic deformation conditions. Wu and Koul (Wu 2010; Wu and Koul, 1995) modified the Langdon's GBS model to develop a constitutive rate equation for GBS in the presence of grain boundary precipitates by incorporating physically defined back stresses opposing dislocation glide and climb. They further concluded that the grain size dependence of the creep rate was grain boundary precipitate distribution dependent. They refined their theoretical model to consider GBS at serrated grain boundaries, using the dynamics of grain boundary dislocation pile-ups, by averaging the sliding rate over the characteristic dimensions of grain boundary serrations. Grain boundary sliding can be accommodated by two mechanism, namely by dislocation activity and by diffusion (Wu, 2010; Wu and Koul, 1995; Xu, et. al., 1999; Wu, Dickson and Koul, 1998).

4. DMM CONSTRUCTION AND ANALYSIS

A modified DMM is constructed between normalized stress (tensile stress /elastic modulus) as the y-axis and homologous temperature (T/T_m, T_m is melting temperature) as the x-axis. A Matlab code developed for this work is used for the construction of Ti alloy DMM. Fig. 2 display the part of the DMM of our interest.

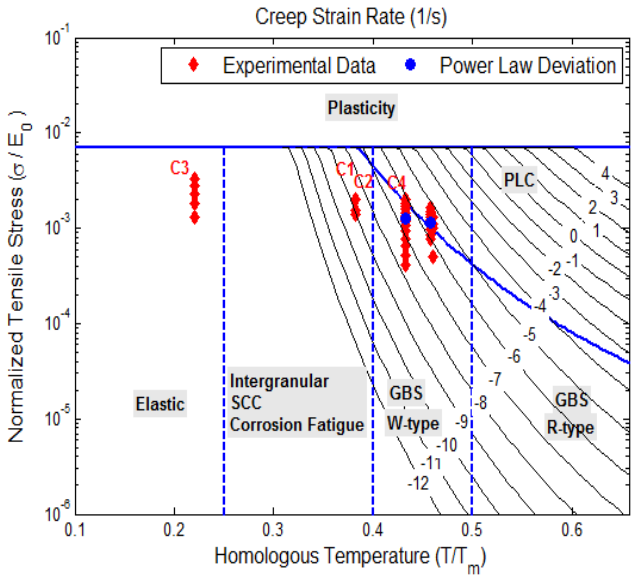

Figure 2. PLC-GBS regime of DMM for Titanium alloy as emerged out of the present simulation work. ♦ Symbols (in red) are the experimental data points from literatures [Badea et. al, 2014; Evans and Harrison, 1983; Nono et. al., 2006; Barboza, Neto, Silva, 2004)]. ● Symbols (in blue) are the power law deviation data points as computed from experimental data.

The data used is given in a separate section (table 1). In view of the application range of the alloy, our interest is in the T/Tm limit up to 0.65 and so the diffusional creep mechanism like bulk (Nabbarro-Herring) and boundary (Coble) diffusions and Harper-Dorn creep are not considered (Fig.1). As indicated earlier, two separate modules are considered and discussed separately. Plots and results under the following modules are integrated finally.

a) Power law creep (PLC) and
b) Grain boundary sliding (GBS)

The strain rate range considered here varies from 10^{4} to 10^{-12} while the homologous temperature range considered is from

0.10 to 0.65. The higher temperature regime above T/T_m =0.4 is dominated by GBS mechanisms and depending on stress and temperature, IG creep fracture occurs by nucleation, growth and linking of voids. Two cavitation damage and cracking mechanisms are generally observed and known as wedge (W) type and round/elliptical (r) type (Campbell, 2012). The distinction between the two are primarily based on geometrical shape. W-type cracks initiate along grain boundaries aligned in shear, while r-type form along grain boundaries in tension. W-types are associated with cracks at triple points due to GBS. W-types tend to form at relatively higher stress, lower temperature and larger grain size. Though no specific temperature-stress regimes are specified in literatures in view of a large number of influencing factors, an arbitrary demarcation line is chosen here at T/Tm=0.50 to distinguish between two dominating creep cavitation damages under GBS.

4.1. Ideal Shear Strength

Ideal strength of solids or upper limit varies widely depending on interatomic bond strength, modulus, temperature etc. Theoretical strength of solids is defined as the ultimate strength beyond which plastic deformation, fracture, or decohesion would occur. A number of theoretical models are developed to explain the ideal strength of materials. Some of models displayed enormous differences with the actual strength of materials, like Frenkel's and Orowan's models (Frenkel, 1926; Orowan, 1948). In our analysis, in DMM a line at the top is always marked to indicate a region where ideal materials collapse. This line is shown in Fig. 2 at normalized value of $7x10^{-3}$ on y-axis.

4.2. Newton-Raphson Simulation

Newton-Raphson method for solving equations numerically is used in this work. It is based on the simple idea of linear approximation with a starting root value of x. The method is a powerful iterative process and follow a set guideline to approximate one root of a function of the form f(x) =0. An initial guess for the root we are trying to find needs to be assumed first , and we call this as initial guess, x. A large number of simulation studies performed with various values of x, strain rates and temperature and iteration number in order to arrive at a converged value of normalized stress on y-axis. The normalized stress is estimated as the ratio of applied tensile stress to elastic modulus.

In our approach, we have focussed on simulations with two differential equations and these are for PLC and GBS as given in Table 1. The parameters and the values considered are also shown.

4.3. Power Law Creep (PLC) Module

Simulation work is performed using Newton Raphson method for the power law creep using the respective constitutive equations as given in Table 1. Small adjustment in the assumed values of x was required in some of the strain rate contour lines. Simulations were carried out for each strain rate from the starting T/T_m as may be seen in Fig. 2. Strain rates from 10^4 to 10^{-12} are considered in this work. The PLC line for strain maximum lies at the top, while the line for lowest strain rate lies at the bottom.

4.4. Grain Boundary Sliding Module

Major plastic deformation mechanisms at medium temperature (0.4) and above are considered to be slip, grain boundary sliding (GBS) and diffusional creep. These tend to occur simultaneously or sequentially and the damage is accumulative. Slip and diffusional creep generally results under higher and lower stress levels respectively, but GBS contributes to plastic deformation at all grain size alloys (Wadsworth et. al, 1999). At finer grain sizes, GBS tends to be the dominant ones. GBS accommodation can occur by the glide or climb of dislocation. A GBS model for creep at elevated temperature is introduced in which accommodation by slip is controlled by lattice diffusion. The simple form of GBS dependency on stress level, grain size and diffusion rate is shown below (Wadsworth et. al, 1999).

$\dot{\varepsilon} = A\,(D_L / d^2)\,\sigma^2$ for GBS by lattice controlled and

$\dot{\varepsilon} = A\,(D_{gb} / d^3)\,\sigma^2$ GBS by grain boundary controlled

where d is the grain size, D is diffusion rate, σ is the stress.

4.5. PLC-GBS Transition

By equating the constitutive equations as given in Table 1 for PLC and grain boundary sliding (GBS) mechanisms, a transition line between the two mechanisms, namely PLC and GBS are outlined as shown in Fig.2. As may be seen, T/Tm above 0.40, the GBS regime is further subdivided into two, namely W type and R type cracking mechanisms. It is assumed in this work that R-type void formation begins at T/Tm greater than 0.50 (Fig. 2).

5. INTEGRATED DMM

The deformation modules as discussed in earlier sections need to be integrated to produce the complete deformation mechanism map for Ti alloys covering wide ranges of stress, temperature and strain rates. The modules integrated DMM is displayed in Fig. 2. Elastic range is typically assumed to dominate below T/T_m =0.25, while failures dominated by SCC, corrosion fatigue etc., expected to fall over $0.25<T/T_m<0.40$.As may be seen in Fig. 2, GBS mechanisms dominates above T/T_m greater than 0.40.

5.1. Alloy Data for Ti-64

Material data from several sources is used in this work for titanium alloy system and this is tabulated in table 1. These data are shown in respect of mechanisms considered for Ti-

alloy components, namely power law creep and grain boundary sliding. (Janghorban and Esmaeili, 1991; Bano, Koul and Nganbe, 2014). The table also show the constitutive equations used for each of the module mechanisms.

Table 1: Ti alloy data for Deformation Mechanism Map

Parameter	Value
Power law creep (climb), $\dot{\varepsilon} = A_{PLC}\frac{D_v Eb}{kT}\left(\frac{\sigma_s-\sigma_b}{E}\right)^n$	
Stress exp. n	4.3
Dorn constant, A_{PLC}	2.382x 10^{18}
Act. Energy for vol. diffusion, Q_v	501 KJ/mol
Pre exponential constant, D_{ov}	3.26 x 10^{-4}
Power law breakdown ($\sigma_s \backslash E_0$)	3.5 x10^{-3}
Grain Boundary sliding, $\dot{\varepsilon}_{GBS} = A_{GBS}\frac{D_{gb}Eb}{kT}\left(\frac{b}{a}\right)^2\left(\frac{\sigma_s}{E}\right)^2$	
Constant, A_{GBS}	6.259x 10^6
Act Energy for GBS, Q_{gb}	311 KJ/mol
Pre exp const, D_{ogb}	3.26x 10^{-4}
Stress exponent, n	2.2
Grain size, a	10 microns

5.2. Experimental Validation

The model based DMM is validated using experimental data points. A survey of literatures was made earlier to look for relevant creep deformation data for the titanium alloy (Badea et. al., 2014, Barboza et.al., 2004, Seco et. al., 2001). A recent work clearly demonstrate a transition in stress exponent values(n) with stress over a temperature range from 450°C to 600°C and stress from 100 to 500Mpa. For stress lower than 0.9x yield strength (YS), steady-state creep strain rate dependency with stress follows a power law close to diffusion model (n ≈ 4-6). For stress higher than 0.9xYS, a power law breakdown domain is observed when n becomes high around (n= 11-22). Similar result was also reported for 500°C and 600°C for Ti-64 alloy (Nono et. al., 2006; Barboza, Neto, Silva, 2004). At low stress, the value of n is 4.2 while n becomes around 8.9 at higher stress indication the power law deviation. These results are collected and suitably converted for x and y axis and shown on the DMM maps in Fig. 2. The experimental points corresponding to the transition region lie scattered, though most transition points are largely close to the predicted boundary between PLC and GBS regimes.

6. DISCUSSION

In view of the wide ranging microstructures expected in α-β Ti alloys and the various creep mechanisms and models reported for steady state creep regime in Ti alloys, an attempt is made here to develop some general relationships among them. The discussion here is presented in the light of four experimental cases (C1…C4) for validation of the model. Fig. 3 represents a typical α-β micrograph of the alloy in mill annealed (MA) condition after creep testing along and consequences of creep deformation at the alpha-beta interfaces and at alpha grains triple points. High triaxiality at triple points induces crack formation. The beta annealed Ti-64 alloy was tested at 455°C (T/Tm = 0.38), at a normalized stress level of 4.25x10^{-3} and at strain rate at 2.8x10^{-5} s^{-1} (Seco et. al., 2001).

At T/T_m of 0.38, referring to Fig. 2, a combination of dislocation creep (PLC) and GBS is perhaps the rate controlling mechanism. This test case is marked as C1 in Fig. 2. Failures occurred by the mechanism of creep cracking and coalescence in the MA alloy.

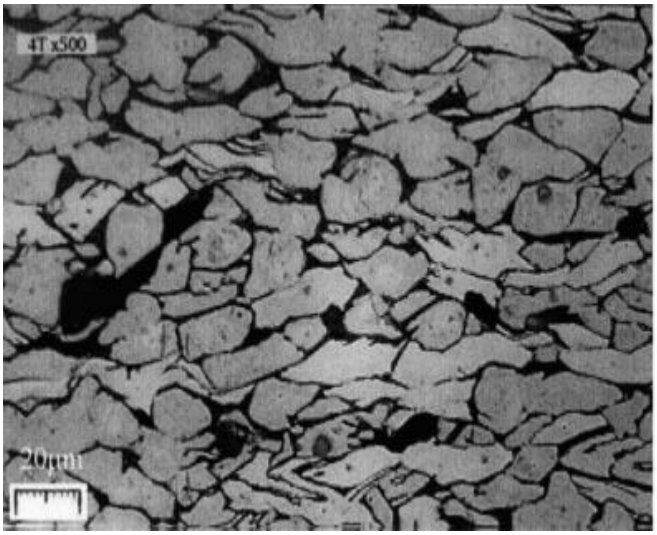

Figure 3. SEM micrograph showing extensive creep cavities formed during creep. Cavities tend to grow normal to principal loading direction (Seco and Irisarri, 2001)

Metallographic analysis confirmed microcracks generated at the former beta grain boundary, that now delineate the colonies of alpha needles and at triple points. This is demonstrated in Fig. 4. The creep test condition was T/Tm equals to 0.38, normalized stress of 4.25x10^{-3} and minimum strain rate observed was 1.3x$10^{-7}$$s^{-1}$. This case is marked as C2 on Fig. 2. However, our theoretical strain lines are somewhat deviated from the position. One prime reason for this is the large differences in grain sizes. The comparison is relatively qualitative. In this case, GBS is the rate controlling mechanism.

The steady state creep rates are lowered as the volume fraction of α-phase increases and the creep rates generally assume lower values with an increasing average grain size (Barbouza et. al 2006, Ro et. al 1989, Chakraborty et. al 1980). Effects of compositions and volume fractions of α and β phases on the overall flow behavior of mill-annealed,

recrystallization-annealed and β-annealed Ti–6Al–4V were studied earlier (Sastry et. al., 1980). Widmanstatten α/β interfaces act as obstacles to dislocation motion. The relatively large initial average grain size of 395 μm decreases the creep rate due to a reduction in grain boundary sliding, dislocation sources and the rate of oxygen diffusion along the grain boundaries (Barbouza et. al., 2006). The testing conditions for above discussion refers to homologous temperature of 0.22, applied normalized stress of 5-10x 10^{-3} and creep steady state strain rate around 2-6x10^{-8} s^{-1}. The creep test temperature was low enough to fall in the elastic region as marked C3 on Fig.2. In this case, the specimen simply deforms heavily and eventually fails.

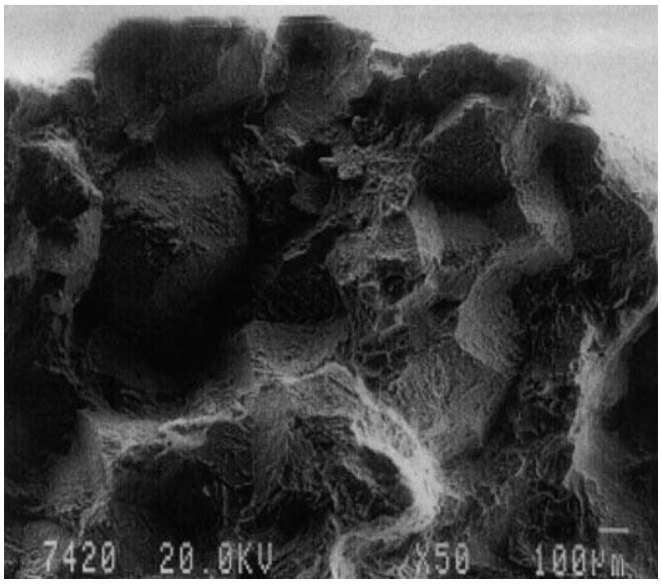

Figure 4. SEM fracture morphology for crept beta annealed Ti64 samples showing IG morphology (Seco and Irisarri, 2001)

Dependency of creep rates on microstructure has also been attributed to the colony size, spheroidization of the β films for the near α alloys. The dislocation substructures deformed at 200 MPa and 550°C at 10^{-2} show the formation of a stable dislocation configuration in the primary α grains leading to cell formation in IMI834. In near α alloy, microstructural and fractographic analysis revealed creep fracture by nucleation, growth and coalescence of cracks nucleated at primary α / transformed β (matrix) interfaces (Fig. 5(a)) (Omprakash et. al. 2010). Microcracks form, by fracture of primary α particles at the specimen surface in bimodal microstructure. The growth and inter linkage of both surface microcracks and interior cracks is controlled by creep deformation of the surrounding region and eventually leads to creep crack growth as illustrated in Fig. 5(b) (Omprakash et al 2010). The test conditions for this case (C4) is as follows: $T/T_m = 0.43$, normalized stress =1.7x10^{-3} and strain rate around 10^{-2}sec^{-1}. The dislocation substructures deformed at 200 MPa and 550°C to a strain of 10^{-2} s^{-1} show the formation of a stable dislocation configuration in the primary α grains leading to cell formation in IMI834 (Es-Soumi, 2001). Presence of fine microstructure and presence of primary α phase and a fully transformed β structure resulted in a higher creep resistance in IMI834. Climb controlled dislocation creep (PLC) in the α phase is proposed as the creep mechanism in the near α alloy. As the future work, effects of grain size on the predicted mechanisms map and comparison with experimental findings will be interesting.

7. SUMMARY

Simulations with Matlab software code are performed in order to obtain contours lines for power law creep and grain boundary sliding deformation mechanisms for a titanium alloy. The study aims to develop a PLC and GBS based damage accumulation processes over strain rates ranging from 10^{4} to 10^{-12} per second over the homologous temperature range of 0.10 to 0.655. A deformation mechanism map is

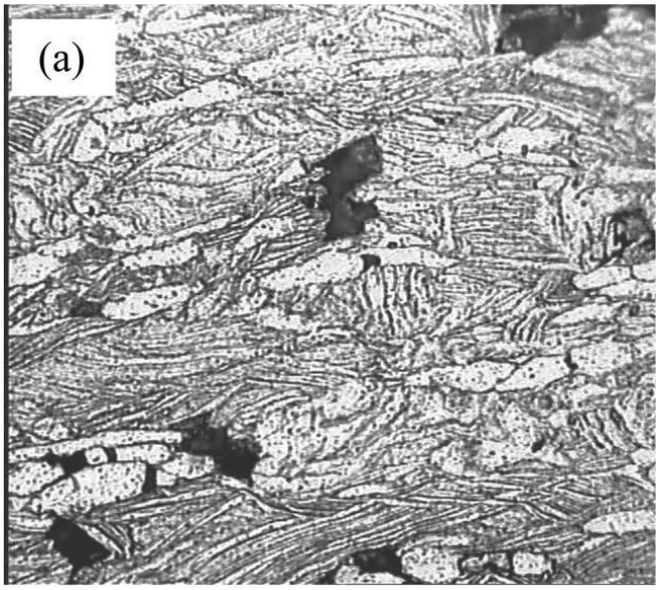

Figure 5(a). Illustration of wedge type (W type) crack formation at primary α- transformed β-phase and elongated grains observed in the near α-Ti alloy (Omprakash et. al., 2010).

generated for alpha-beta Ti alloy of 10 micron grain size. Two dominating mechanisms, namely a) Power law creep and c) Grain boundary sliding accommodated by different processes are considered. Appropriate constitutive equations are used for two mechanisms and simulation work is performed using the Newton- Raphson method. The modified and reconstructed map is validated using experimental data points. The experimental points support the theoretical

contours lines over the homologous temperature ranges 0.40 to 0.50. Four experimental validation cases are discussed in the context of predicted map of creep deformations. The test cases support the predicted map reasonably well in view of large differences in grain sizes and other structural conditions.

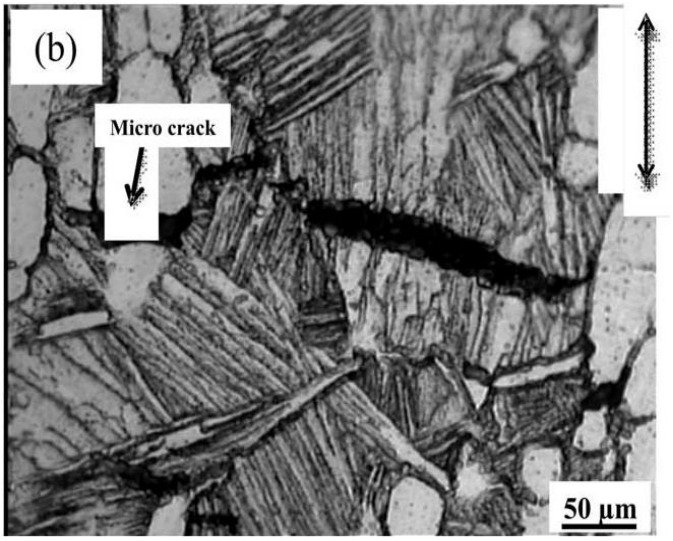

Figure 5(b). Formation and linkage of microcracks at the primary α particles observed in crept fracture surface of near α-Ti alloy (Omprakash et. al., 2010).

REFERENCES

Badea L., Surand M., Ruau J., Viguier B. (2014). *Creep Behavior of Ti-6Al-4V from 450°C to 600°C*, U.P.B. Sci. Bull., Series B, Vol. 76, Iss. 1, ISSN 1454 – 2331.

Evans W. J. and Harrison G. F (1983). P*ower law steady state creep in α/β titanium alloys*, Journal of Materials science, 18, 3449-3455.

Seco F. J., Irisarri A. M. (2001). *Creep failure Mechanisms of a Ti-6Al-4V thick plate*, Fatigue and Fracture of Engineering Materials &Structures, Volume 24, Issue 11, pp. 741–750.

Frost H. J., and Ashby M. F. (1982). *Deformation-Mechanism Maps, The Plasticity and Creep of Metals and Ceramics*, by Cambridge University, Permagon Press.

Langdon T. G. (2006). *Grain boundary sliding revisited: Developments in sliding over four decades***,** J Mater. Sci. **41** (2006) 597–609.

Janghorban K, Esmaeili, S. (1991). *Deformation mechanism map for Ti-6wt%Al alloy*, Journal of Materials science 26, 3362 -3365.

Briguente, L. A. N. S., Couto, A. A., Guimarães, N. M. Reis, D. A. P, C., Neto, M. and Barboza, M. J. R, (2012), *Determination of Creep Parameters of Ti-6Al-4V with Bimodal and Equiaxed Microstructure*, Defect and Diffusion Forum Vols. 326-328 (2012) pp 520-524 (2012), Trans Tech Publications, Switzerland doi:10.4028/www.scientific.net/DDF.326-328.520

Bano N., Koul A. K, Nganbe M. (2014). *A Deformation Mechanism Map for the 1.23Cr-1.2Mo-0.26V Rotor Steel and Its Verification Using Neural Networks*, Metallurgical and Materials Transactions, 45A, 2.

Banerjee A., Zhao J., Koul A. K, Kumar A., Srivastava A., Goel N. (2013). *Physics-Based Prognostics for LCF Crack Nucleation Life of IMI 685 Aero-engine Compressor Disc*, Procee. Annual conference of prognostics and health management.

Metzger, M. and Seifert, T. (2012). *A Mechanism-Based Model for LCF/HCF and TMF/HCF Life Prediction: Multiaxial Formulation, Finite-Element Implementation and Application to Cast Iron*", TECHNISCHE MECHANIK, 32, 2-5.

Lütjering, G., Williams, J., C. (2007). *Titanium Engineering Materials and Processes*, Second ed. Springer.

Matthew J. Donachie, Jr. (2002). Selection of titanium alloys for design, Chap. 6, Handbook of Materials selection, ed. Myer Kutz, John Wiley & Sons, NY.

Leyens, C., Peters, M. (ed.), (2003). *Titanium and Titanium Alloys - Fundamentals and Applications*, WileyVCH Verlag GmbH & Co. KGaA.

Peters, M. Hemptenmacher, J., Kumpert J. and Leyens C. (2003). *Structure and properties of Titanium and Titanium alloys*, ed. C. Leyens, M. Peters, 2003, Wiley-VCH Verlag GMBH &co.

Es-Souni, M. (2001). *Creep behaviour and creep microstructures of a high-temperature titanium alloy Ti–5.8Al–4.0Sn–3.5Zr–0.7Nb–0.35Si–0.06C (Timetal 834), Part I. Primary and steady-state creep*, Materials Characterization 46, 365– 379

Es-Souni, M. (2001). *Creep Deformation Behavior of Three High-Temperature near α-Ti Alloys: IMI 834, IMI 829, and IMI 685*, Metallurgical and Materials Transactions A, Volume 32, Number 2, pp. 285-293(9)

Wu, X. J. (2010). *Life prediction of gas turbine materials*, http://cdn.intechopen.com/pdfs-wm/12091.pdf.

Wu X. J. and A.K. Koul (1995). Metall. Mater. Trans. A, vol. 26A, pp. 905–14.

Xu, S., Wu, X .J. and Koul A. K. (1999). Metall. Mater. Trans. A, vol. 30A, pp. 1039–45.

Xu S., Dickson, J. I. and Koul, A. K (1998). Metall. Mater. Trans. A, vol. 29A, pp. 2687–95.

Frenkel, J., (1926). Z. Phys. 37, 572.

Orowan E., (1948). Rep. Prog. Phys., 12, 183

Wadsworth, J., Ruano, O.A., Sherby O. D., (1999). *Deformation by Grain Boundary Sliding and Slip Creep versus Diffusional Creep*", The Minerals, Metals and Materials (TMS) Annual Meeting , 4.

Barboza, M. J. R., Perez, E. A. C, Medeiros, M. M., Reis, D.A. P., Nono, M. C. A., Neto, F. P., Silva, C. R. M. (2006). *Creep Behavior of Ti-6Al-4V and a Comparison*

with Titanium Matrix Composites, Materials Science and Engineering, 428, pp. 319-326.

F C Campbell (2012) Fatigue and Fracture- Understanding the basics ASM International, The Materials information society

M J R Barboza, CM Neto and CRM Silva (2004). *Creep mechanisms and physical modeling for Ti-6Al-4V*, Materials science and engineering, vol. A, 369, p. 201.

Y. Ro, S. Nakazawa, H. Onodera, K. Ohno, T. Yamagata, I. Tomizuka, M. Yamazaki, ISIJ Int. 29 (1989) 165–170.

A.K. Chakrabarti, E.S. Nichols, in: H. Kimura, O. Izumi (1980). Titanium Science and Technology, vol. 2, Metall. Soc. AIME, Kyoto.

S.M.L. Sastry, P.S. Pao, K.K. Sankaran, in: H. Kimura, O. Izumi (Eds.), Titanium Science and Technology, vol. 2.
Metall. Soc. AIME, Kyoto, 1980, pp. 873–886.

C.M. Omprakash, D.V.V. Satyanarayana and Vikas Kumar (2010). "*Effect of microstructure on creep and creep crack growth behaviour of titanium alloy*" Transactions of The Indian Institute of Metals, Vol 63, 1-2, pp 457-2010

S. Suri, T. Neeraj, G.S. Daehn, D.-H. Hou, J.M. Scott, R.W. Hayes, M.J. Mills (1997). "*Mechanisms of primary creep in α/β titanium alloys at lower temperatures*", Materials Science and Engineering A234-236, 996-999

BIOGRAPHIES

Dr. Amar Kumar has more than 25 years of research and consulting experience in the fields of structural materials characterization and development, fracture mechanics, failure analysis and applications. Dr. Kumar is currently working as senior research scientist in the R&D project of diagnostics, prognostics and health management of aeroengine components. He specializes in both data driven approaches and physics-based modeling and simulations.

Alka Srivastava graduated with a B.A.Sc. (Electrical Engineering) from the University of Ottawa. She joined Nortel Networks in 1990 as a Member of Scientific Staff. She joined Tecsis Corporation in 2003 as a member of the Research and Development team. Her research interests are in the areas of project management, software quality assurance, fault tolerant computing, numerical analysis and statistical methods.

Nita Goel graduated with a B.E. (Electronics & Telecommunications in 1985 from the University of Jodhpur, India. She completed her M.A.Sc (Electrical Engineering) from the University of Ottawa in 1994. She founded Tecsis Corporation in 1994 and is currently engaged in Research and Development. Her research interests are in the areas of software engineering, fault tolerant computing, numerical analysis and statistical methods.

Dr. Avi Banerjee is the Systems Development and Services Manager at Life Prediction Technologies Inc. He manages the development of diagnostics and prognostics tools for turbo-machinery and avionics at LPTi. His broad areas of research interest are performing physics based prognostics case studies, ENSIP, data trending for failure prediction, development of parts life tracking systems and the development of PHM framework. He works extensively with end users requiring prognostics services. Dr. Banerjee is a registered professional engineer in Ontario, Canada.

Dr. Ashok Koul is the President of Life Prediction Technologies Inc. (LPTi), Ottawa, ON and also acts as an overall technical advisor. He has 25 years of experience in the field of materials engineering and life prediction with extensive experience in managing and supervising research and development activities in gas turbine structures, materials and life cycle management strategies. Over the years he has made key contributions in identifying and applying existing as well as emerging technologies in the field of gas turbine engineering.